

# Warm H<sub>2</sub>O and OH in the disk around the Herbig star HD 163296

D. Fedele<sup>1</sup>, S. Bruderer<sup>1</sup>, E.F. van Dishoeck<sup>1,2</sup>, G.J. Herczeg<sup>3</sup>, N.J. Evans II<sup>4</sup>, J. Bouwman<sup>5</sup>, Th. Henning<sup>5</sup>, J. Green<sup>4</sup>

<sup>1</sup> Max Planck Institut für Extraterrestrische Physik, Giessenbachstrasse 1, 85748 Garching, Germany;

<sup>2</sup> Leiden Observatory, PO Box 9513, 2300 RA Leiden, The Netherlands;

<sup>3</sup> Kavli Institute for Astronomy and Astrophysics, Yi He Yuan Lu 5, Beijing, 100871, P.R. China;

<sup>4</sup> University of Texas at Austin, Department of Astronomy, 2515 Speedway, Stop C1400, Austin TX 78712-1205, USA;

<sup>5</sup> Max Planck Institute for Astronomy, Königstuhl 17, 69117, Heidelberg, Germany

Received May 16 2012; accepted July 17 2012

## ABSTRACT

We present observations of far-infrared (50–200  $\mu\text{m}$ ) OH and H<sub>2</sub>O emission of the disk around the Herbig Ae star HD 163296 obtained with *Herschel*/PACS in the context of the DIGIT key program. In addition to strong [O I] emission, a number of OH doublets and a few weak highly excited lines of H<sub>2</sub>O are detected. The presence of warm H<sub>2</sub>O in this Herbig disk is confirmed by a line stacking analysis, enabled by the full PACS spectral scan, and by lines seen in *Spitzer* data. The line fluxes are analyzed using an LTE slab model including line opacity. The H<sub>2</sub>O column density is  $10^{14} - 10^{15} \text{ cm}^{-2}$ , and the excitation temperature is 200–300 K implying warm gas with a density  $n > 10^5 \text{ cm}^{-3}$ . For OH we find  $N_{\text{mol}}$  of  $10^{14} - 10^{15} \text{ cm}^{-2}$  and  $T_{\text{ex}} \sim 300\text{--}500 \text{ K}$ . For both species we find an emitting region of  $r \sim 15 - 20 \text{ AU}$  from the star. We argue that the molecular emission arises from the protoplanetary disk rather than from an outflow. This far-infrared detection of both H<sub>2</sub>O and OH contrasts with near- and mid-infrared observations, which have generally found a lack of water in the inner disk around Herbig AeBe stars due to strong photodissociation of H<sub>2</sub>O. Given the similarity in column density and emitting region, OH and H<sub>2</sub>O emission seems to arise from an upper layer of the disk atmosphere of HD 163296, probing a new reservoir of water. The slightly lower temperature of H<sub>2</sub>O compared to OH suggests a vertical stratification of the molecular gas with OH located higher and H<sub>2</sub>O deeper in the disk, consistent with thermo-chemical models.

**Key words.** Protoplanetary disks – Stars: formation

## 1. Introduction

Water is a key molecule for the chemical and physical evolution of protoplanetary disks. Together with O and OH, it forms the main reservoir of oxygen. The formation of water ice layers on dust grains may improve their sticking behaviour and thereby help the coagulation process towards larger particles that ultimately leads to the formation of planetesimals and planets. The growth of icy grains is also likely involved in the delivery of water to planets. Recent observations at near- ( $\sim 3 \mu\text{m}$ ) and mid-infrared ( $\sim 10\text{--}30 \mu\text{m}$ ) wavelengths have revealed the common presence of hot ( $T \sim 500\text{--}1000 \text{ K}$ ) water and OH vapor in the atmosphere of T Tauri disks (Salyk et al. 2008; Carr & Najita 2008; Pontoppidan et al. 2010; Mandell et al. 2012). In contrast, disks around the more massive Herbig AeBe stars do not show hot water vapor emission and appear to be depleted in water molecules (Mandell et al. 2008; Pontoppidan et al. 2010; Fedele et al. 2011). A likely explanation is that hot water is photodissociated by the stronger ultraviolet radiation emitted by the Herbig stars in the regions of the disks ( $< \text{a few AU}$ ) probed at these wavelengths (e.g. Fedele et al. 2011). Indeed, in the case of the young eruptive star EX Lupi the H<sub>2</sub>O emission is variable as a consequence of the changing UV radiation field (Banzatti et al. 2012).

However, cooler water may survive further out or deeper into these disks, but that region can only be probed by longer wavelength data. *Herschel* offers the opportunity to search for these water lines with high sensitivity. Detections of water in disks with *Herschel* have been reported by Hogerheijde et al. (2011) using HIFI and Riviere-Marichalar et al. (2011) using PACS, but these observations refer only to disks around T Tauri stars.

In this letter we report the detection of OH far-infrared emission lines and the signal of warm H<sub>2</sub>O toward the Herbig Ae star HD 163296 (A1V) at a distance of  $d = 118 \text{ pc}$  (van Leeuwen 2007). The star is isolated with no evidence of a stellar companion and is surrounded by a well-studied disk (e.g., Mannings & Sargent 1997; Grady et al. 2001; Isella et al. 2007). A bipolar microjet and a series of Herbig-Haro knots are observed at optical and UV wavelengths perpendicular to the disk (e.g., Wassell et al. 2006). The disk has recently been modeled by Tilling et al. (2012), who also report upper limits on selected OH and H<sub>2</sub>O lines from PACS data obtained in the GASPS *Herschel* key program.

## 2. Observations and data reduction

HD 163296 was observed on April 03 2011 with the PACS instrument (Poglitsch et al. 2010) onboard the *Herschel Space Observatory* (Pilbratt et al. 2010) as part of the DIGIT key program (*KPOT\_nevans\_1*, PI: N. Evans). The target was observed in SED mode covering the wavelength range 50–220  $\mu\text{m}$  with

Send offprint requests to: Davide Fedele,  
e-mail: fedele1e@mpe.mpg.de

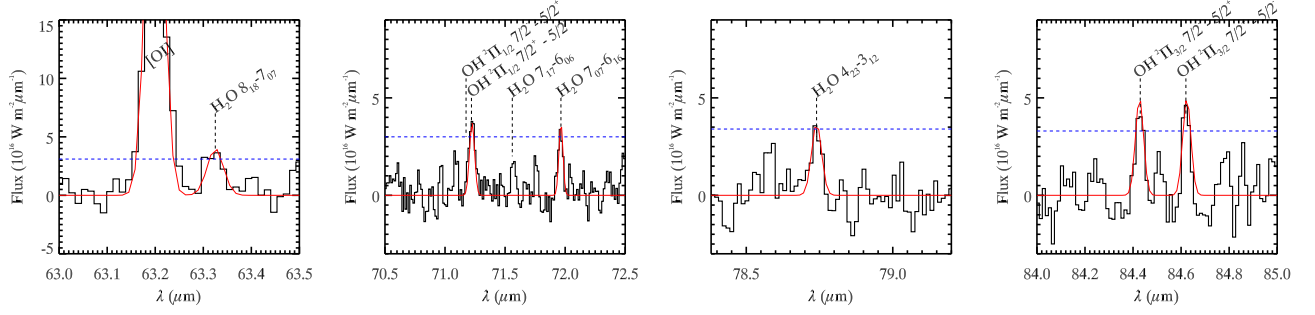


**Fig. 1.** PACS spectrum (continuum-subtracted) of selected lines. The (blue) dashed line indicates the r.m.s. of the baseline multiplied by 3. The presented spectrum has been smoothed (smooth width = 2 bins) for clarity. The red line is a Gaussian fit to the detected lines.

$R \sim 1000 - 3000$  (obsid: 1342217819, 1342217829). The observations were carried out in chopping/nodding mode with a chopping throw of  $6''$ . The total on-source integration time is 6176 seconds for the B2A (51-73  $\mu\text{m}$ ) and short R1 (70-105  $\mu\text{m}$ ) modules and 8360 seconds for the B2B (70-105  $\mu\text{m}$ ) and long R1 (140-220  $\mu\text{m}$ ) modules. The data have been reduced with HIPE 8.0.2489 with standard calibration files from level 0 to level 2. The two nod positions were reduced separately (oversampling factor = 3, up-sampling factor = 1 to ensure that the noise in each spectral point is independent) and averaged after a flat-field correction.

The spectrum has been extracted from the central spaxel (9.4'' square) to optimize the signal-to-noise ( $S/N$ ) ratio. Due to the large point spread function of the telescope, some flux leaks into the other spaxels of the PACS array. To recover the absolute flux level, we apply a correction factor using the spectrum extracted from the central 9 spaxels (3x3 extraction): this is performed by fitting a 3<sup>rd</sup>-order polynomial to two spectra (central spaxel and 3x3), the conversion factor is the ratio between the 2 fits. Finally, the spectrum is scaled so that the spectrum matches the PACS photometry (from Meeus et al. in preparation) at 70  $\mu\text{m}$  and 160  $\mu\text{m}$ .

The line flux ( $F_{\text{line}}$ ) was measured by fitting a Gaussian function and the uncertainty ( $\sigma$ ) is given by the product  $STD_F \sqrt{\delta\lambda FWHM^2}$ , where  $STD_F$  ( $\text{W m}^{-2} \mu\text{m}^{-1}$ ) is the standard deviation of the (local) spectrum,  $\delta\lambda$  is the wavelength spacing of the bins ( $\mu\text{m}$ ) and  $FWHM$  is the full width half maximum of the line ( $\mu\text{m}$ ).

### 3. Results

We clearly detect the strong [O I] 63  $\mu\text{m}$  line as well as 5 OH far-infrared features above  $3\sigma$  (i.e. having  $F_{\text{line}}/\sigma > 3$ , Table 1). Spectra of selected lines are shown in Fig. 1. The OH lines are readily recognized because of their doublet pattern; only intra-ladder transitions, which have the largest Einstein-A coefficients, are found. In the case of the  $^2\Pi_{1/2} 7/2-5/2$  doublet at 71  $\mu\text{m}$  only one of the two lines is detected, although the non-detection of the second line is hardly significant within the noise. Asymmetric line intensities of  $\Lambda$ -doublets are predicted at high temperature (Offer & van Dishoeck 1992), but because of the noise this doublet is not considered in our further analysis.

Three lines of H<sub>2</sub>O are detected slightly above  $3\sigma$  (Table 2). The H<sub>2</sub>O  $8_{18} - 7_{07}$  line at 63.32  $\mu\text{m}$  is seen not only in our data

**Table 1.** [O I] and OH line fluxes.

Transition	$\lambda_{\text{obs}}$ ( $\mu\text{m}$ )	$F_{\text{line}}$ ( $10^{-17} \text{ W m}^{-2}$ )	$F_{\text{line}}^m$ ( $10^{-17} \text{ W m}^{-2}$ )	$E_u$ (K)	$\log A_{ul}$ ( $\text{s}^{-1}$ )
[O I]	63.2	$19.8 \pm 1.2$		228	-4.05
$^2\Pi_{1/2} 9/2^+ - 7/2^-$	55.8	$5.6 \pm 1.1$	6.7	875	0.34
$^2\Pi_{1/2} 9/2^- - 7/2^+$	55.9	$6.1 \pm 1.1$	6.7	875	0.34
$^2\Pi_{3/2} 9/2^- - 7/2^+{}^a$	65.1	$6.4 \pm 1.2$	5.9	512	0.11
$^2\Pi_{3/2} 9/2^+ - 7/2^-$	65.2	$5.8 \pm 1.0$	5.9	511	0.10
$^2\Pi_{3/2} 7/2^- - 5/2^+$	84.6	$2.2 \pm 0.4$	2.8	291	-0.28
$^2\Pi_{3/2} 7/2^+ - 5/2^-$	84.4	$2.2 \pm 0.4$	2.8	291	-0.28
$^2\Pi_{3/2} 5/2^- - 3/2^+$	119.2	$1.2 \pm 0.3$	0.9	121	-0.86
$^2\Pi_{3/2} 5/2^+ - 3/2^-$	119.4	$0.9 \pm 0.3$	0.9	121	-0.86

**Notes.** Column  $F_{\text{line}}^m$  reports the line flux predicted by the best-fit model.

<sup>(a)</sup> Blended with o-H<sub>2</sub>O  $6_{25}-5_{14}$ .

**Table 2.** H<sub>2</sub>O line fluxes.

Transition	$\lambda_{\text{obs}}$ ( $\mu\text{m}$ )	$F_{\text{line}}$ ( $10^{-17} \text{ W m}^{-2}$ )	$F_{\text{line}}^m$ ( $10^{-17} \text{ W m}^{-2}$ )	$E_u$ (K)	$\log A_{ul}$ ( $\text{s}^{-1}$ )
p-H <sub>2</sub> O $4_{31}-3_{22}$ <sup>a</sup>	56.31	$2.7 \pm 1.6$	2.5	552	0.16
o-H <sub>2</sub> O $9_{09}-8_{18}$ <sup>a</sup>	56.82	$0.9 \pm 1.6$	1.5	1323	0.39
o-H <sub>2</sub> O $8_{18}-7_{07}$	63.32	$2.0 \pm 0.6$	2.0	1070	0.24
o-H <sub>2</sub> O $7_{07}-6_{16}$	71.95	$2.2 \pm 0.5$	1.9	843	0.06
o-H <sub>2</sub> O $4_{23}-3_{12}$	78.74	$1.8 \pm 0.4$	1.7	432	-0.32
o-H <sub>2</sub> O $6_{16}-5_{05}$ <sup>a</sup>	82.03	$0.8 \pm 0.8$	1.5	643	0.06
p-H <sub>2</sub> O $3_{22}-2_{11}$ <sup>a</sup>	89.98	$0.9 \pm 0.9$	0.8	296	-0.45
o-H <sub>2</sub> O $2_{21}-1_{10}$ <sup>a</sup>	108.07	$0.7 \pm 0.5$	0.7	194	-0.59
o-H <sub>2</sub> O $4_{14}-3_{03}$ <sup>a</sup>	113.54	$0.7 \pm 0.4$	0.6	323	-0.61

**Notes.** <sup>(a)</sup> Flux integrated over 5 bins centered at the expected line position.

but also in the GASPS spectrum shown by Tilling et al. (2012) although they do not claim the detection. The H<sub>2</sub>O  $4_{23} - 3_{12}$  line at 78.74  $\mu\text{m}$  is seen here with a flux of  $1.8 (\pm 0.4) 10^{-17} \text{ W m}^{-2}$  while Tilling et al. (2012) report only a  $3\sigma$  upper limit of  $1.5 10^{-17} \text{ W m}^{-2}$ . Meeus et al. (2012) recently claim a detection of far-infrared H<sub>2</sub>O emission towards this source based on new GASPS data. Pontoppidan et al. (2010) also provide tentative detections of H<sub>2</sub>O lines in the mid-infrared *Spitzer* wavelength range. Table 2 summarizes our fluxes and includes the fluxes measured at the position of some (undetected) key H<sub>2</sub>O lines that are used later in the analysis.

The detected lines have upper level energies over a wide range with  $E_u/k \sim 120 - 900$  K (OH) and  $E_u/k \sim 400 - 1300$

<sup>1</sup> This formula comes directly from the error propagation of the sum  $\Sigma_i(F_i)$ , where  $F_i$  is the flux of the  $i$ -th spectral bin.

K (H<sub>2</sub>O). Most of the lines are detected in the blue part of the spectrum.

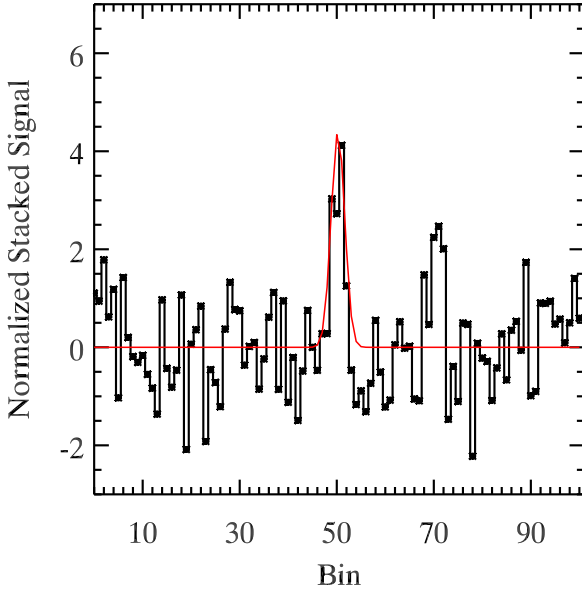


**Fig. 2.** Stacking of 54 H<sub>2</sub>O lines. Water emission is clearly detected in the stacked spectrum. The integrated signal is  $S_{\text{H}_2\text{O}} = 7\sigma$ .

### 3.1. Confirmation of H<sub>2</sub>O by line stacking

Since only 3 H<sub>2</sub>O lines are marginally detected above  $3\sigma$ , we have used the availability of the full DIGIT PACS spectrum to confirm the presence of warm water in this disk through a stacking analysis. Line stacking is commonly done in extra-galactic surveys to detect the faint emission lines from the outer regions of galaxies (e.g., Schrubba et al. 2011). Warm water has many lines spread throughout the far-infrared wavelength region which can be used for this purpose. In this work, we stacked spectra centered at the location of different H<sub>2</sub>O lines based on the far-infrared lines detected with PACS towards the protostar NGC 1333 IRAS 4B (Herczeg et al. 2012). The 95–100  $\mu\text{m}$  range is excluded because of spectral leakage (produced by overlap of grating orders). Blended lines are excluded from this analysis and OH and [O I] lines are masked. The remaining number of H<sub>2</sub>O lines available for the analysis is 54. The stacked spectrum is the weighted average of 54 spectra, each of which is 100 bins wide centered at the position of a water line:  $F = \frac{\sum_{j=1}^{54} w_j F_j}{\sum_{j=1}^{54} w_j}$  where  $F_j$  is the (continuum-subtracted) spectrum centered at the  $j$ -th water line and  $w_j$  is the weight of the line. The weight corresponds to  $STD_j^{-1}$ , where  $STD_j$  is the standard deviation of the continuum-subtracted spectrum  $F_j$ . The lines are stacked by bin because the spectral resolution in velocity space varies but is approximately constant in bins.

The stacked spectrum is shown in Fig. 2. The warm H<sub>2</sub>O signal is clearly detected and centered on the central bin. The integrated H<sub>2</sub>O signal is 7 times its uncertainty. The false alarm probability (FAP), i.e. the probability to detect a  $7\sigma$  signal by stacking random portions of the PACS spectrum, is  $< 0.03\%$  based on 10,000 randomized tests (see Appendix B).

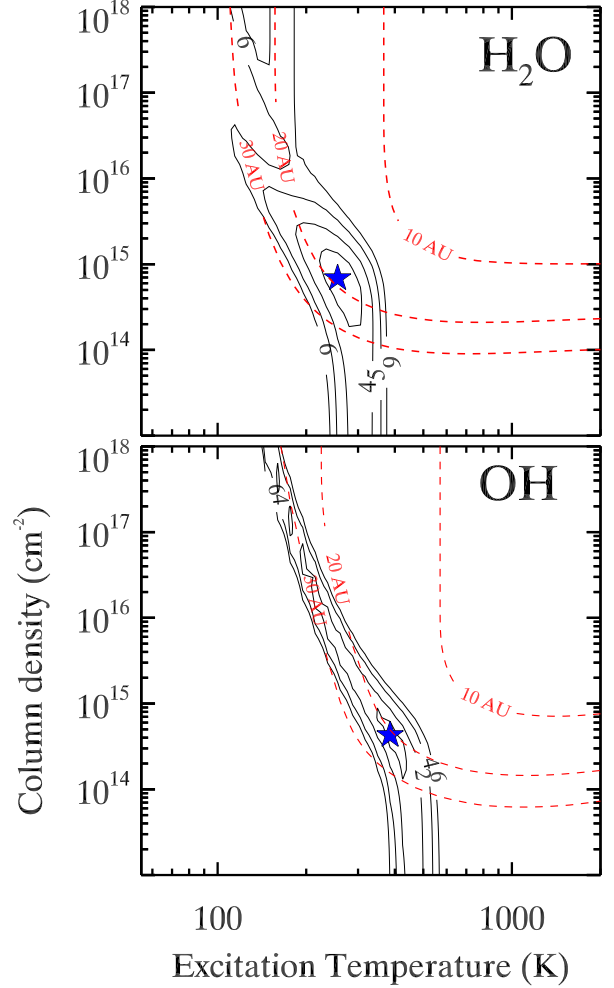


**Fig. 3.** Contours of the reduced  $\chi^2$  for the slab/LTE model for H<sub>2</sub>O (upper panel) and OH (lower panel). The value of the reduced  $\chi^2$  is overplotted. The (red) dashed lines provide the radius of the emitting region (10, 20, 30 AU). The star indicates the location of the minimum  $\chi^2$ .

This analysis confirms the presence of warm H<sub>2</sub>O in the PACS spectrum of HD 163296. Stacking H<sub>2</sub>O lines separately in spectra from the two nod positions also yields  $> 3\sigma$  detections. The H<sub>2</sub>O signal is only detected in the central spaxel and not in off-source spaxels. These last two tests exclude the contamination from an extended and/or off-source emission and confirm that the H<sub>2</sub>O lines detected in the PACS spectrum are associated with HD 163296.

## 4. Analysis

In this section we analyze the OH and H<sub>2</sub>O excitation using a uniform slab of gas in local thermal equilibrium (LTE) including the effect of line opacity (see Appendix A for details). The limited number of lines and their large uncertainties do not warrant a more sophisticated non-LTE treatment. The analysis is based on the data in Tables 1 and 2, including the mid-infrared lines detected with *Spitzer*/IRS (Pontoppidan et al. 2010). Free parameters of the model are the excitation temperature  $T_{\text{ex}}$  (K) and the molecular column density  $N_{\text{mol}}$  ( $\text{cm}^{-2}$ ). The size of the emitting

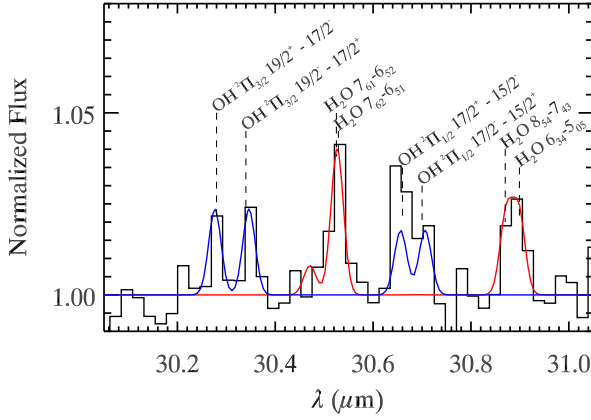


**Fig. 4.** *Spitzer*/IRS spectrum (continuum-subtracted) of selected lines. The red and blue lines are the best model for H<sub>2</sub>O and OH respectively.

region, given by its radius  $r$ , is not a free parameter since it can be determined uniquely for every given combination of  $T_{\text{ex}}$  and  $N_{\text{mol}}$ . Comparison between models and data is done based on reduced  $\chi^2$  values.

The range of models that yields an acceptable agreement is shown in Fig. 3. Overplotted are contours for the radius  $r$ . For H<sub>2</sub>O, the data are best fitted ( $1\sigma$ ,  $p = 68.3\%$ ) by models with  $T_{\text{ex}} \sim 200 - 350$  K and  $N_{\text{mol}} \sim 10^{14} - 10^{16} \text{ cm}^{-2}$  and  $r \sim 15 - 20$  AU. For OH, the data are best fitted for  $N_{\text{mol}} \sim 10^{14} - 10^{15} \text{ cm}^{-2}$ ,  $T_{\text{ex}} \sim 300 - 500$  K and  $r \sim 20$  AU. The *Spitzer*/IRS spectrum of selected lines is shown in Fig. 4 along with the best model.

Further constraints to the H<sub>2</sub>O column density and temperature come from individual line flux ratios. In particular, the ratio between far- and mid-infrared lines (e.g.  $7_{07} - 6_{16}/7_{61} - 6_{52}$ ) constrains the column density to  $> 10^{14} \text{ cm}^{-2}$ . On the other hand, the ratio  $8_{18} - 7_{07}/8_{08} - 7_{17}$  constrain the upper limit of the H<sub>2</sub>O column density to  $2 \times 10^{15} \text{ cm}^{-2}$ . We also note that models with higher column density produce several H<sub>2</sub>O lines which are not detected in the PACS and IRS spectra. The ratio  $8_{18} - 7_{07}/9_{09} - 8_{18}$  constrains the temperature to  $< 300$  K.

## 5. Discussion

The primary result of this Letter is a detected signal of H<sub>2</sub>O toward a Herbig star, in addition to OH. The H<sub>2</sub>O emitting region is found to be 15-20 AU, demonstrating that H<sub>2</sub>O can survive the UV radiation further away from the star while it is likely photodissociated in the inner part of the disk.

Given that a bipolar microjet is known to be associated with HD 163296 (Wassell et al. 2006), the question arises whether the far-infrared molecular line emission presented here indeed arises from the disk or whether it comes from such a jet. There are several arguments in favor of the disk. First, we note that HD 163296 is isolated and not associated with a molecular cloud. No evidence of a molecular outflow has been reported to date (e.g. Bae et al. 2011). Second, the spectrally resolved CO  $J = 3 - 2$  line in the sub-millimeter shows the characteristic double-peaked profile for gas in Keplerian rotation (Thi et al. 2001; Dent et al. 2005). At much shorter wavelengths ( $4.7 \mu\text{m}$ ), the CO ro-vibrational emission lines are also characterized by a double-peaked profile (Salyk et al. 2011). Thus, there is no hint of any significant small- or large-scale molecular outflow in these data that could dominate the PACS emission. Third, the

PACS data show no evidence for extended/off-source emission beyond the central spaxel, not even for the strong [O I]  $63 \mu\text{m}$  line, which places the warm H<sub>2</sub>O within 500 AU of the central star.

The inferred OH and H<sub>2</sub>O excitation temperatures of several hundred K indicate warm emitting regions. The high critical densities of the H<sub>2</sub>O lines,  $n_c \geq 10^7 \text{ cm}^{-3}$ , implies that the density of the gas should also be high ( $n \gtrsim 10^5 \text{ cm}^{-3}$ , e.g. Herczeg et al. 2012). These conditions and the arguments above suggest that the OH and H<sub>2</sub>O emission arises from the atmosphere of the disk associated with HD 163296 at radial distances  $> 10$  AU from the star.

Assuming that the OH/H<sub>2</sub>O far-infrared lines are emitted by the disk, which zone does this emission trace? Models of the water chemistry in Herbig disks suggest at least three chemically distinct zones (e.g., Woitke et al. 2009; Glassgold et al. 2009; Walsh et al. 2010, 2012; Vasyunin et al. 2011; Najita et al. 2011): (i) an inner disk water reservoir ( $\lesssim$  few AU) with a chemistry close to LTE; (ii) a cold water belt at large distances ( $\gtrsim 50$  AU) where gaseous H<sub>2</sub>O results primarily from photodesorption of water ice; and (iii) a hot water layer at intermediate distances of 1–30 AU and at medium heights with water formation driven by high temperature neutral-neutral reactions. The derived parameters for our OH and H<sub>2</sub>O lines are consistent with zone (iii) (see also Tilling et al. 2012); zone (i) is probed by the near-infrared data and zone (ii) can be targeted by HIFI observations of low- $J$  lines. Thus, the PACS data reveal a new water reservoir in disks.

## 6. Conclusions

We have presented new Herschel/PACS observations of the disk around the Herbig Ae star HD 163296. We obtain detections of far-infrared lines of warm OH and H<sub>2</sub>O toward a Herbig star. The presence of warm H<sub>2</sub>O is confirmed by a line stacking analysis ( $7\sigma$  detection) enabled by the full PACS spectral scan. The LTE slab model analysis including optical depth effects indicates emission from the intermediate radii of the disk. Combined with near-infrared and sub-millimeter data, the oxygen chemistry can now be probed over the entire disk range.

## References

- Bae, J.-H., Kim, K.-T., Youn, S.-Y., et al. 2011, *ApJS*, 196, 21
- Banzatti, A., Meyer, M. R., Bruderer, S., et al. 2012, *ApJ*, 745, 90
- Carr, J. S. & Najita, J. R. 2008, *Science*, 319, 1504
- Dent, W. R. F., Greaves, J. S., & Coulson, I. M. 2005, *MNRAS*, 359, 663
- Fedele, D., Pascucci, I., Brittain, S., et al. 2011, *ApJ*, 732, 106
- Glassgold, A. E., Meijerink, R., & Najita, J. R. 2009, *ApJ*, 701, 142
- Grady, C. A., Polomski, E. F., Henning, T., et al. 2001, *AJ*, 122, 3396
- Herczeg, G. J., Karska, A., Bruderer, S., et al. 2012, *A&A*, 540, A84
- Hogerheijde, M. R., Bergin, E. A., Brinch, C., et al. 2011, *Science*, 334, 338
- Isella, A., Testi, L., Natta, A., et al. 2007, *A&A*, 469, 213
- Mandell, A. M., Bast, J., van Dishoeck, E. F., et al. 2012, *ApJ*, 747, 92
- Mandell, A. M., Mumma, M. J., Blake, G. A., et al. 2008, *ApJ*, 681, L25
- Mannings, V. & Sargent, A. I. 1997, *ApJ*, 490, 792
- Meeus, G., Montesinos, B., Mendigutia, I., et al. 2012, *ArXiv e-prints*
- Najita, J. R., Ádámkóvics, M., & Glassgold, A. E. 2011, *ApJ*, 743, 147
- Offer, A. R. & van Dishoeck, E. F. 1992, *MNRAS*, 257, 377
- Pilbratt, G. L., Riedinger, J. R., Passvogel, T., et al. 2010, *A&A*, 518, L1
- Poglitsch, A., Waelkens, C., Geis, N., et al. 2010, *A&A*, 518, L2
- Pontoppidan, K. M., Salyk, C., Blake, G. A., et al. 2010, *ApJ*, 720, 887
- Riviere-Marichalar, P., Ménard, F., Thi, W. F., et al. 2011, *ArXiv e-prints*
- Salyk, C., Blake, G. A., Boogert, A. C. A., & Brown, J. M. 2011, *ApJ*, 743, 112
- Salyk, C., Pontoppidan, K. M., Blake, G. A., et al. 2008, *ApJ*, 676, L49
- Schruba, A., Leroy, A. K., Walter, F., et al. 2011, *AJ*, 142, 37
- Thi, W. F., van Dishoeck, E. F., Blake, G. A., et al. 2001, *ApJ*, 561, 1074

- Tilling, I., Woitke, P., Meeus, G., et al. 2012, A&A, 538, A20  
van der Tak, F. F. S., Black, J. H., Schöier, F. L., Jansen, D. J., & van Dishoeck, E. F. 2007, A&A, 468, 627  
van Leeuwen, F. 2007, A&A, 474, 653  
Vasyunin, A. I., Wiebe, D. S., Birnstiel, T., et al. 2011, ApJ, 727, 76  
Walsh, C., Millar, T. J., & Nomura, H. 2010, ApJ, 722, 1607  
Walsh, C., Nomura, H., Millar, T. J., & Aikawa, Y. 2012, ApJ, 747, 114  
Wassell, E. J., Grady, C. A., Woodgate, B., Kimble, R. A., & Bruhweiler, F. C. 2006, ApJ, 650, 985  
Woitke, P., Kamp, I., & Thi, W. 2009, A&A, 501, 383

## Appendix A: Slab model

For an optically thin line from a point-like source, the flux can be written by

$$F_{ul} = d\Omega_s \cdot I_{ul} = d\Omega_s \frac{h\nu_{ul}}{4\pi} A_{ul} N_{\text{mol}} \frac{g_u e^{-E_u/kT}}{Q(T)} \quad (\text{A.1})$$

with the solid angle of the source  $d\Omega_s$ , the line frequency  $\nu_{ul}$ , the Einstein-A coefficient  $A_{ul}$ , the molecular column density  $N_{\text{mol}}$ , the statistical weight of the upper level  $g_u$ , the energy of the upper level  $E_u$  and the partition function  $Q(T)$ . The solid angle of the emitting region can be written as  $d\Omega_s \equiv \pi r^2/d^2$ , with the radius of the emitting region  $r$  and a distance of  $d = 118$  pc to HD 163296. For an optically thick line, the integrated intensity is obtained from

$$I_{ul} = \Delta\nu \frac{\nu_{ul}}{c} B_{\nu_{ul}}(T_{\text{ex}})(1 - e^{-\tau_{ul}}) . \quad (\text{A.2})$$

with the opacity at the line center

$$\tau_{ul} = \frac{A_{ul}c^3}{8\pi\nu_{ul}^3\Delta\nu} \left( N_l \frac{g_u}{g_l} - N_u \right) . \quad (\text{A.3})$$

The (thermal) width of the lines is assumed to be  $\Delta\nu \sim 1$  km s<sup>-1</sup>, appropriate for gas at several hundred K and we assume a simple square like line profile as e.g. used in the RADEX code (van der Tak et al. 2007).

## Appendix B: False alarm probability of water detection in the stacked spectrum

We performed a simulation to measure the probability to detect a signal with an integrated value,  $S > 7\sigma$ . This provides the false alarm probability (FAP) of the detection in the stacked spectrum. We performed 10,000 random stackings of 54 (equal to the number of water lines) parts of the PACS spectrum of HD 163296. After 10,000 iterations we measured the distribution of the ratio of the integrated signal over its uncertainty (measured as in Sec. 3.1). We mask the bins containing H<sub>2</sub>O, OH and [O I] emission. Fig. B.1 shows the distribution of  $S/\sigma$ . The distribution is well fitted by a Gauss function (red line,  $\tilde{\chi}^2 = 0.03$ ), centered (as expected) at  $S/\sigma = 0$  (i.e. an equal number of positive and negative peaks). The number of occurrences with  $S/\sigma > 7$  is  $< 3$ , which corresponds to FAP  $< 0.03\%$  according to Bayesian statistics.

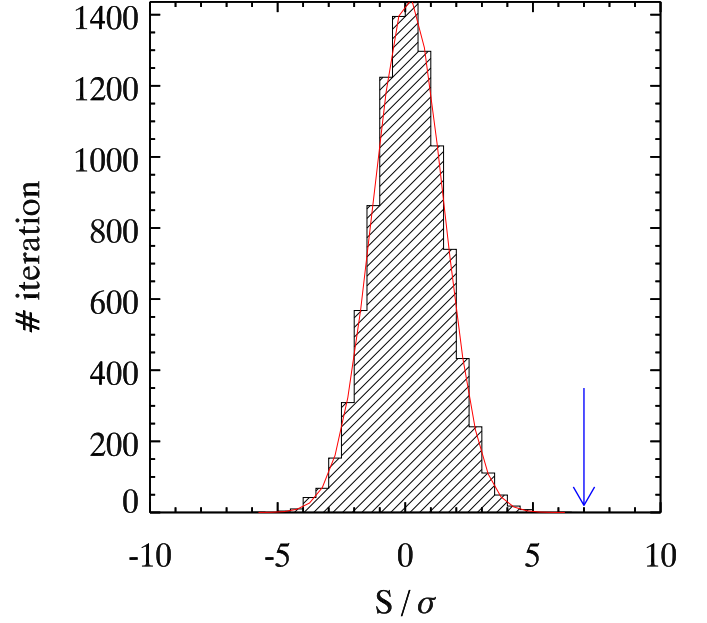


**Fig. B.1.** Distribution of  $S/\sigma$  after 10,000 random stackings of 54 parts of the PACS spectrum of HD 163296. The red line shows the Gaussian fit. The arrow indicates the location of the H<sub>2</sub>O signal (Fig. 2).